

PLAGIOCLASE IN PRIMARY MINERALOGY OF ANCIENT CRUST, NORTHERN HELLAS, MARS.

M.S. Phillips¹, C.E. Viviano², and J.E. Moersch¹, ¹Department of Earth and Planetary Sciences, University of Tennessee, Knoxville, TN 37996-1526 (mphill58@vols.utk.edu), ²Johns Hopkins University Applied Physics Lab, Laurel, MD 20723.

Introduction: The earliest stable crusts of rocky bodies, including Mars, possibly formed via differentiation from magma oceans [e.g., 1, 2]. Characterizing the igneous mineralogy of primary crust can, therefore, help constrain early mantle conditions. Older than ~3.8 Ga, Argyre, Hellas, and Isidis basins are three of the largest and best-preserved impact structures on Mars. Surrounding these basins in discontinuous annuli are km-scale blocks of crust exhumed from depth during the impact events [3]. In this study, we used Compact Reconnaissance Imaging Spectrometer for Mars (CRISM) mapping data to characterize the primary igneous mineralogy associated with ancient crustal outcrops exposed in uplifted massifs north of Hellas basin, as part of a larger effort to characterize such outcrops around all three basins: Argyre, Hellas, and Isidis.

Geologic Background: Hellas basin (centered at ~42° S, 70° E) is the largest unambiguous impact structure on Mars (D ~2300 km). The ~4 Ga impact exhumed deep crustal materials and likely upper mantle rocks [4, 5]. Crustal thinning and extension caused structural uplift circumferential to the basin, exposing deeply buried material in mountainous blocks referred to as, “uplifted massifs”[6]. These massifs provide a window into the deepest crust, and likely the upper mantle (e.g., [3]). Such material is useful for constraining early mantle composition both explicitly (if of mantle origin) and implicitly as fractionated derivatives of mantle. Promontories of other genuses, such as volcanic constructs, remnant dikes, and remnant crater materials (walls, rims, and central peak complexes) also occur on the northern Hellas rim and must be distinguished from uplifted massifs.

Data and Methods: To differentiate possible uplifted massifs from other topographic promontories along the Hellas rim, we used the Thermal

Emission Imaging System (THEMIS) Day IR 100 m/pixel global base map with the global Context Camera (CTX) ~5 m/pixel mosaic [7]. Uplifted massifs were identified as km- to 10's-of-km-sized cohesive ($TI > \sim 350 \text{ J m}^{-2} \text{ K}^{-1} \text{ s}^{1/2}$) massive and fractured blocks, commonly basin-concentric dip slopes, arcuate and/or rounded peaks, high relative topographic relief (typically > 2-4 km), and often overlain by poorly to well stratified regolith. Volcanic constructs were identified as high-standing, conical/domical structures with possible associated calderas at the cap and flows around the base. Dikes were identified as high-standing linear features, commonly forming complexes or radially to volcanic constructs. Remnant craters were identified based on their arcuate to circular morphology. Remnant craters can be difficult to distinguish from uplifted massifs modified by impacts, however. In cases of uncertain identification, we categorized promontories as “possible uplifted massif”.

Mineral identifications were made as part of a larger mapping campaign in the Tyrrhena Terra region, using CRISM 200 m/pixel multispectral mapping data to identify igneous and alteration minerals. Customized add-on tools for the Environment for Visualizing Images (ENVI) were used for analyses. Geomorphologic mapping of massifs was done in ArcGIS. Mineral identifications that overlapped uplifted massifs, or possible uplifted massifs, were extracted for this study.

Results: We identified 188 outcrops with plagioclase, olivine, or pyroxene spectral signatures in northern Hellas massifs (Fig. 1, top panel). Olivine and low-calcium pyroxene (LCP) were the most common minerals with 129 and 128 locations identified, respectively. Plagioclase and high-calcium pyroxene (HCP) were the least numerous with 97 and 34 locations identified, respectively. The minerals appear correlated with distance from the Hellas center

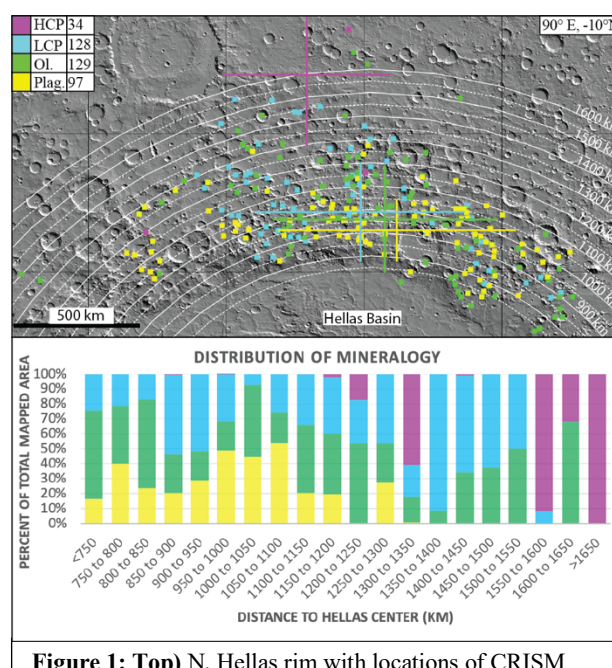


Figure 1: Top N. Hellas rim with locations of CRISM identifications. Concentric arcs show distance to Hellas center. **Bottom** Histogram of the areal fraction of uplifted massifs identified as each mineral per radial bin. Note the general decrease of plagioclase, and increase of pyroxene with distance from the Hellas center

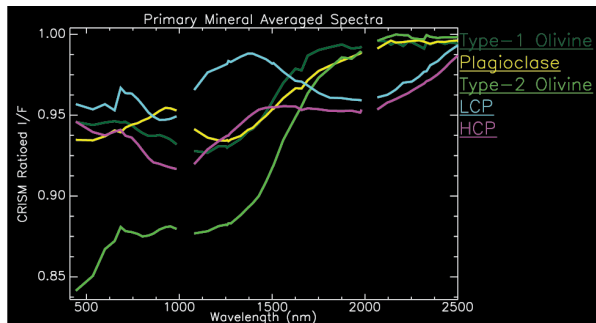


Figure 2: Average CRISM spectra of primary igneous minerals identified in this study. Spectra were normalized to their maximum value for ease of viewing. See text for description of Type-1 vs. Type-2 olivine. Gaps in the spectra are due to removal of atmospheric noise.

(Fig. 1, bottom panel). Plagioclase and olivine occur closer to the Hellas center than LCP and HCP. LCP is more common than HCP, consistent with previous studies that indicate a prevalence of LCP in older terrains compared to higher proportions of HCP in younger lava flows [e.g., 8].

Representative spectra (averages, $N \geq 15$) of each primary mineral in this study are shown in figure 2. Olivine is separated into Type-1 and Type-2, indicating a difference in the breadth and depth of the $\sim 1 \mu\text{m}$ absorption feature. Here, we use Type-1 to indicate olivine with a narrower $1\text{-}\mu\text{m}$ feature, and Type-2 to indicate olivine with a broader $\sim 1\text{-}\mu\text{m}$ feature with a continuum-removed center that falls at longer wavelengths. This difference can be attributed to variability in Fe-content (where Fe-rich olivines yield a broader absorption, i.e., Type-2) [e.g., 9]. However, other variables cause a broadening of the $\sim 1\text{-}\mu\text{m}$ absorption feature, such as larger grain size and higher sub-pixel abundance [10].

Discussion: The radial position of material on a basin rim is indicative of its pre-impact position, either directly if the mechanism of exhumation is structural uplift, or in an inverted manner if the material is ejecta [11]. The observed radial distribution of minerals along the northern Hellas rim in uplifted massifs, therefore, indicates a possible pre-impact stratigraphy representative of original layering.

An unexpected amount of plagioclase was detected in uplifted massifs. The plagioclase absorption feature, centered around $1.25 \mu\text{m}$ (Fig. 2), results from a crystal field effect caused by substitution of minor amounts of Fe^{2+} (≥ 0.05 wt. %), likely for Ca^{2+} , into octahedral sites [12, 13]. Laboratory experiments indicate the VSWIR plagioclase feature is detectable when the mineral has sufficient Fe-content [12] and is in high abundance ($>85\%$) [14], as is commonly the case for lunar anorthosites [15]. Although plagioclase is the most common mineral on Mars' surface [e.g., 16], its detection in the Visible to Short-Wavelength Infrared (VSWIR) is rare

because it most frequently occurs in basalt, and the absorption feature is easily obfuscated when plagioclase is intimately mixed with mafic minerals (e.g., pyroxene or olivine) [e.g., 14], and, possibly, because there is not sufficient Fe^{2+} substitution to cause an absorption. Plagioclase may also be detected at lower modal abundances ($\geq 50\%$) if the matrix is spectrally bland [17], such as in felsic rocks, or if its grain size is large ($\sim 840 \mu\text{m}$) [18]; examples include Archean megacrystic anorthite-bearing dikes and hypabyssal intrusions [19], Galapagos plagioclase-phyric basalts [20], and plagioclase-phyric dikes in Iceland [21]. Other lithologies possibly consistent with VSWIR detections of plagioclase include plagioclase sandstone, plagioclase-phyric andesite, and tephra deposits.

Several identifications of plagioclase have recently been made with CRISM in study areas adjacent to [22, 18], and overlapping with [23] our study. Previous interpretations of feldspathic outcrops are felsic [22], anorthositic [23], and plagioclase-phyric basaltic [18]. Our results greatly expand the number of feldspathic outcrops identified. An assessment of the multiple working hypotheses for the lithologic interpretation of our plagioclase detections will help constrain the petrogenesis of these outcrops and the evolution of the early Martian mantle, including possible magma ocean environments.

Magma ocean scenarios potentially consistent with production of a feldspathic component to the early crust are: 1) a deeply-sourced melt produced by cumulate overturn of a whole mantle magma ocean, or 2) a shallow magma ocean [e.g., 24]. We plan to expand our survey to uplifted massifs around Argyre and Isidis basins, to analyze the spatial distribution of identified mineralogy, and to further analyze the nature of feldspathic outcrops. The spatial distribution of ancient crustal minerals may help constrain the geometry of a putative mantle overturn and subsequent crustal production [e.g., 10].

References: [1] Solomatov, V., 2007. [2] Borg, L. E. and Draper, D. S., Met. & Plan. Science, 2003, **38**(12) [3] Tanaka, K. L., 2005. [4] Tanaka, K. L. and Leonard, G. J., JGR, 1995, **100**(E3) [5] Koeppen, W. C. and Hamilton, V. E., JGR-Planets, 2008, **113**(E5) [6] Leonard, G. J. and Tanaka, K. L., 2001. [7] Dickson, J. L., et al., LPSC, 2018. [8] Grott, M., et al., Space Sci. Rev., 2013, **174**(1-4) [9] Viviano-Beck, C. E., et al., JGR-Planets, 2014, **119**(6) [10] Ody, A., et al., JGR-Planets, 2013, **118**(2) [11] Melosh, H. J., 1989. [12] Adams, J. B. and Goulaud, L. H., LPSC, 1978, (9) [13] Burns, R. G., 1993. [14] Serventi, G., et al., Icarus, 2013, **226**(1) [15] Makiko, O., et al., Nature, 2009, **461**(7261) [16] Bandfield, J. L., et al., Science, 2000, **287**(5458) [17] Metelka, V., et al., J. of African Earth Sci., 2015, **112** [18] Rogers, A. D. and Nekvasil, H., GRL, 2015, **42**(8) [19] Ashwal, L. D., 1993. [20] Cullen, A., et al., J. of Volc. and Geothermal Res., 1989, **37**(3-4) [21] Óskarsson, B. V., et al., J. of Volc. and Geothermal Res., 2017, **332** [22] Wray, J. J., et al., Nat Geosci, 2013, **6**(12) [23] Carter, J. and Poulet, F., Nat Geosci, 2013, **6**(12) [24] Elkins-Tanton, L. T., et al., JGR-Planets, 2005, **110**(E12)